

Location of Mn(II) ions in manganese aluminophosphate molecular sieves: a comparative study of MnAPO-11 and MnAPO-41

A.K. Sinha, C.V.V. Satyanarayana, D. Srinivas, S. Sivasanker, P. Ratnasamy *

National Chemical Laboratory, Pune 411 008, India

Received 15 April 1999; received in revised form 8 June 1999; accepted for publication 9 June 1999

Dedicated to the late Werner O. Haag in appreciation of his outstanding contributions to heterogeneous catalysis and zeolite science

Abstract

Manganese-incorporated aluminophosphate molecular sieves, MnAPO-11, MnAPO-41 and MnSAPO-41, were prepared by hydrothermal methods. The samples were characterized by the techniques of X-ray diffraction (XRD), scanning electron microscopy (SEM), thermogravimetric/differential thermal analysis (TGA/DTA), magic-angle spinning (MAS) nuclear magnetic resonance (NMR) spectroscopy (^{31}P and ^{27}Al) and electron spin resonance (ESR) spectroscopy. Thermal analysis data reveal that complete oxidation of the template takes place at higher temperatures in the manganese-containing samples than in the AlPO_4s . The greater difficulty in template removal from manganese-containing samples is attributed to the presence of protonated template ions compensating the negative charge created by manganese present in the framework. ESR studies reveal that a larger fraction of the manganese in $\text{AlPO}_4\text{-11}$ is present in the framework than in $\text{AlPO}_4\text{-41}$. At least four different Mn^{2+} species in both framework and extra-framework positions could be identified in the samples. © 2000 Elsevier Science B.V. All rights reserved.

Keywords: Aluminophosphates; ESR; Metal aluminophosphates; MnAPO-11; MnAPO-41; MnSAPO-41

1. Introduction

Aluminophosphate ($\text{AlPO}_4\text{-}n$) molecular sieves possess an overall framework neutrality owing to the regular alteration of Al^{3+} and P^{5+} tetrahedra in their structure and consequently little acidity. Brønsted acidity can be generated in these materials by replacing P^{5+} in the framework by Si^{4+} (SAPOs) [1–4] or Al^{3+} by divalent cations (Me^{2+}) such as Mg^{2+} , Co^{2+} , Mn^{2+} and Zn^{2+} (MeAPOs) [5–8]. These isomorphous substituents (Si^{4+} , Me^{2+}) are

usually added to the synthesis gel during the preparation of the SAPOs and MeAPOs, and can be present in different framework and extra-framework locations in the crystalline solids. For example, Si^{4+} ions have been reported to be present in the framework in isolated locations, in patches as ‘ SiO_2 ’ and as ‘ $\text{SiO}_2\text{-AlO}_2$ ’ islands, and in extra-framework positions as isolated ions or amorphous material [5]. The nature of the silicon species present in SAPOs has been found to depend on many parameters such as the silicon content, the method of preparation, the structure of the microporous material and the SiO_2 source used [9]. Although SAPOs have been the most studied and are better understood than MeAPOs, information on the loca-

* Corresponding author. Tel.: +91-20-589-3030; fax: +91-20-589-3355.

E-mail address: prs@ems.ncl.res.in (P. Ratnasamy)

tion of metal ions in many MeAPOs is also available [10–15].

In the case of MnAPO-5, most of the Mn^{2+} ions were found to be present in extra-framework positions and inhomogeneously distributed even at low manganese contents [11]. On the other hand, manganese was incorporated mainly in the framework position in MnAPO-11 and MnAPSO-11 at low manganese levels, the extra-framework component increasing with manganese content [12,13]. In MnAPSO-44, only 15% of the manganese was distributed homogeneously in the framework, the rest being situated in manganese-rich areas at a manganese content of 0.9 at.% [14]. It thus appears that the incorporation of manganese in the framework is related to both the structural aspects of the AlPO_4 system, the manganese loading and probably the preparation procedure. In this paper, we examine the location of manganese in MnAPO-41 and MnAPO-11 and its incorporation from the precursor gels using mainly electron spin resonance (ESR) spectroscopic techniques. Other characterization techniques, such as nuclear magnetic resonance (NMR) spectroscopy, thermogravimetric/differential thermal analysis (TGA/DTA) and X-ray diffraction (XRD), have also been used in the study.

2. Experimental

2.1. Synthesis

Chemicals used for synthesis were orthophosphoric acid (85%, sd fine chem, India), di-*n*-propylamine (DPA, Aldrich), fumed silica (Aerosil-200, Sigma) and manganese acetate tetrahydrate (Aldrich). Aluminium isopropoxide (Aldrich) was the aluminium source for the synthesis of MnAPO-11, whereas pseudoboehmite (Catapal-B, Vista, 74% Al_2O_3) was used for the MnAPO-41 structure. Syntheses were carried out in 120 cm^3 stainless steel autoclaves lined with polytetrafluoroethylene liners under autogeneous pressure without any agitation.

Hydrothermal syntheses of AlPO_4 -41 and MnAPO-41 were carried out based on the method described by Prakash et al. [16], and AlPO_4 -11

and MnAPO-11 were synthesized following the procedure of Messina et al. [17]. The molar compositions of the gels used for the synthesis of various substituted AlPO_4 s are given in Table 1.

To synthesize MnAPO-11, aluminium isopropoxide (11.6 g) was added slowly to 13.0 g of distilled water and the mixture was stirred for 45 min with a mechanical stirrer (REMI, India; 500–600 rev min^{-1}). To this solution dilute orthophosphoric acid (6.0 g in 6.5 g of water) was added dropwise and stirred for 1.5 h. Manganese acetate (2.04 g) was added to this solution and stirred for a further 30 min. Finally, 4.3 g of DPA was added and the mixture was stirred for another 2 h to get a homogeneous gel. This was transferred to an autoclave and heated at 473 K for 24 h. The products were washed with distilled water, dried at 393 K for 12 h, and calcined at 823 K for 16 h by gradually raising the temperature (2 K min^{-1}). Then, 1 g of the calcined sample was stirred in 100 cm^3 of 1 M NaCl solution at 343 K for 5 h to exchange Na^+ for extra-framework manganese.

In a typical synthesis of MnAPO-41, 6.82 g of pseudoboehmite was added slowly to dilute phosphoric acid (15.56 g of H_3PO_4 diluted with 38 g of water) while stirring with a mechanical stirrer (REMI, India; 500–600 rev min^{-1}). The resulting mixture was stirred for 2 h prior to the addition of manganese acetate solution. Subsequently, 20.24 g of DPA was added dropwise under vigorous stirring. After stirring for 2 h, the pH was adjusted to ~ 7.7 , if required, by the addition of a few drops of dilute phosphoric acid. Seed crystals of AlPO_4 -41 (0.5 wt.% of Al_2O_3) were added to the resulting gel and stirred for few minutes. The material was then transferred to an autoclave, and heated for 24 h at 473 K. The preparation procedure for MnSAPO-41 was similar except that silica was added prior to the addition of the template. The product crystals were separated from the mother liquor, washed with water, and dried at 373 K for 12 h. The as-synthesized samples were calcined with a slow rise of temperature to 793 K in nitrogen atmosphere, followed by heating the sample for 16 h in air to remove the template. Four samples of MnAPO-41 (i–iv) with different manganese contents, two samples of MnSAPO-41

Table 1
Synthesis gel ratios and chemical compositions of calcined, manganese-incorporated AlPO_4s

Sample	Synthesis gel ratios (mole)						pH		Chemical composition, crystalline phase			
	MnO	Al_2O_3	P_2O_5	SiO_2	DPA	H_2O	Initial	Final	Mn	Al	P	Si
MnAPO-41(i)	0.003	0.998	1.4	–	4.0	55.0	7.72	9.80	0.001	0.491	0.508	–
MnAPO-41(ii)	0.008	0.995	1.4	–	4.0	55.0	7.74	9.70	0.002	0.495	0.503	–
MnAPO-41(iii)	0.030	0.985	1.4	–	4.0	55.0	7.75	9.84	0.006	0.482	0.514	–
MnAPO-41(iv)	0.050	0.975	1.4	–	4.0	55.0	7.70	9.75	0.009	0.479	0.512	–
MnSAPO-41(i)	0.008	0.995	1.4	0.1	4.0	55.0	7.75	9.60	0.005	0.469	0.476	0.052
MnSAPO-41(ii)	0.030	0.985	1.4	0.1	4.0	55.0	7.74	9.86	0.006	0.456	0.496	0.044
MnAPO-11	0.300	1.0	1.0	–	1.0	50.0	5.3	9.1	0.029	0.480	0.491	–

(i and ii) and a sample of MnAPO-11 were used in these studies (Table 1).

2.2. Chemical composition

For determining the chemical composition, calcined samples were dissolved in aqua regia, diluted in water and used for the estimation of phosphorus and aluminium. The undissolved residue in the case of MnSAPOs was fused with lithium metaborate, dissolved in dilute nitric acid and used for the estimation of silicon by atomic absorption spectrophotometry (AAS; Varian Spectr SF-220). Analysis of phosphorus was carried out by means of inductively coupled plasma-atomic emission spectroscopy (ICP-AES; Perkin-Elmer PE-1000), whereas aluminium was analysed by AAS.

2.3. Measurements

X-ray powder diffraction patterns of the samples were recorded (Rigaku D/Max-Vc diffractometer) using nickel-filtered $\text{Cu K}\alpha$ radiation. Thermogravimetric and differential thermal analyses (TGA and DTA) were carried out (Setaram, TG-DTA 92) in an air flow at a heating rate of 10 K min^{-1} . High-resolution magic-angle spinning (MAS) NMR studies were carried out on a Bruker DRX-500 MHz spectrometer using a single pulse excitation technique. Pulses of $\pi/2$ for ^{31}P and $\pi/12$ for ^{27}Al with acquisition delays of 10 and 1 s, respectively, were used. Standard 7 mm zirconia rotors with spinning speeds of 5–5.5 kHz were employed.

ESR experiments were performed at 298 and 77 K with a Bruker EMX X-band ($\nu \approx 9.75 \text{ GHz}$) spectrometer using 100 kHz field modulation. The microwave frequency was measured with a frequency counter built into the Bruker ER 041 XG-D microwave bridge, with a Gun diode as the source of radiation. DPPH was used as a field marker ($g=2.0036$). Spectral simulations and manipulations were carried out using Bruker WINEPR and SIMFONIA software packages. The spectra were acquired using multiple scan mode whenever required and relative intensities were calculated by double integration of the recorded ESR signal. Measurements at 77 K were done with a finger-type quartz inserting dewar. Spectra of solutions were recorded in an aqueous cell.

Samples were dehydrated by evacuating for 8–9 h at 623 K in suitable home-made EPR cells. Rehydration was done by keeping the calcined samples in a desiccator containing water. All the as-synthesized samples were white while the calcined/hydrated samples, in particular MnAPO-11, MnSAPO-41 and MnAPO-41, containing more manganese, turned pink, indicating the presence of hexa-coordinated manganese attached presumably to some H_2O ligands.

3. Results and discussion

The as-synthesized as well as calcined samples of manganese-substituted -11 and -41 structures were subjected to X-ray diffraction analysis to determine their crystallinity and phase purity. All the samples were found to be highly crystalline

pure phases (Fig. 1), the d -values of which match very well those reported. Although it is common to find small amounts of -11 and -39 structures in the -41 samples, these impurities were not detected (by XRD) in our samples.

Chemical compositions of all the calcined samples, obtained through wet chemical methods, are given in Table 1. Analysis of the results shows that the amount of manganese incorporated in the crystalline material increases with higher amounts of manganese in the gel.

3.1. Thermogravimetric analysis

The TGA/DTA results of the as-synthesized AlPO_4 -11, MnAPO -11, AlPO_4 -41, and

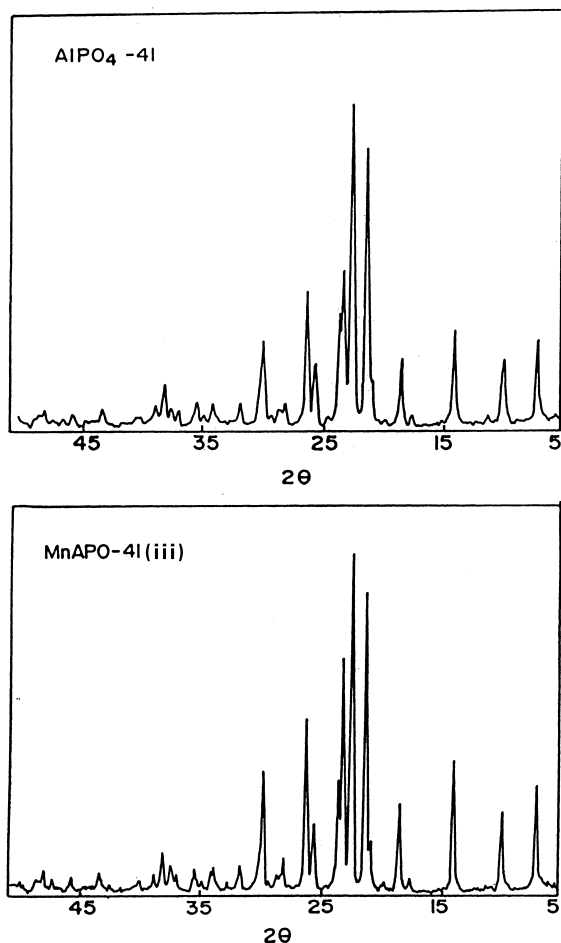


Fig. 1. XRD patterns of (a) AlPO_4 -41 and (b) MnAPO -41(iii).

MnAPO -41(iii) and MnSAPO -41(ii) are presented in Fig. 2 and Table 2. Three stages of weight loss are noticed in the AlPO_4 s: an endothermic stage I in the range 473–573 K (5.5% for AlPO_4 -11 and 6.8% for AlPO_4 -41) and exothermic stages II (1.5% for AlPO_4 -11 and 1.8% for AlPO_4 -41) and III (<1.2% for AlPO_4 -11 and -41) in the ranges 573–723 K and 723–873 K, respectively. Similar TGA/DTA patterns have also been reported by earlier workers for AlPO_4 molecular sieves [18].

In the case of MnAPO samples, additional stages of weight loss, IV and V, in the temperature range 773–973 K are also noticed. Besides, there is a significant reduction in the loss of template in stages I and II and an increase in loss in stage III. This is more noticeable in MnAPO -11 and MnSAPO -41. The studies suggest that the template is removed at a higher temperature from MnAPO -11 and MnSAPO -41 than from MnAPO -41 or the aluminophosphates. The weight loss in stages III to V is associated with strongly interacting, charge-compensating, protonated template species. The S_{BET} values measured for the calcined samples are in the expected range of 180–200 $\text{m}^2 \text{g}^{-1}$, suggesting the absence of pore blockage after calcination.

3.2. MAS NMR

High-resolution solid-state ^{31}P and ^{27}Al MAS NMR spectra of the as-synthesized AlPO_4 -41 and MnAPO -41(iv) samples are given in Fig. 3. The phosphorus spectrum of AlPO_4 -41 shows at least six clearly discernible phosphorus environments at $\delta = -11.5$, -19.5 , -23.8 , -27.5 , -30.4 and -36.1 ppm. On substitution of manganese, only two environments can be clearly seen. Prakash et al. [19,20] investigated the presence of various crystallographically distinct environments in AlPO_4 -41 and its cobalt-, manganese- and silicon-substituted variants. They observed similar chemical shifts in their investigation on AlPO_4 -41 samples as well and assigned the peaks between $\delta = -24$ and -31.5 ppm to crystallographically distinct T sites. The peaks at $\delta = -11.5$ and -19.5 ppm were attributed to defect sites based on ^1H - ^{31}P cross-polarization experiments. Although they did not observe any perceptible changes in the ^{31}P MAS

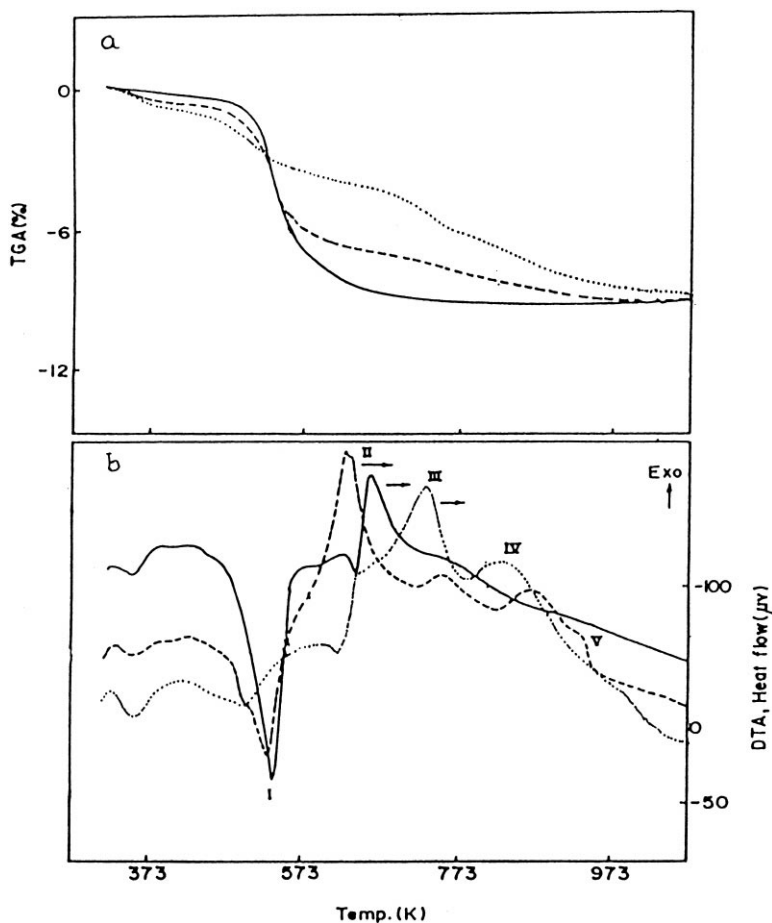


Fig. 2. TGA (a) and DTA (b) profiles of AlPO₄-41 (—), MnAPO-41 (---) and MnSAPO-41 (···).

NMR spectra upon cobalt and manganese incorporation, substitution of silicon led to a coalescence of different phosphorus peaks into a single peak at $\delta = -31.5$ ppm. This change in the phosphorus NMR spectrum was interpreted to imply a change of symmetry in the lattice leading to single phosphorus environments (not resolved by MAS NMR). Our ³¹P NMR spectrum of MnAPO-41 differs from that reported by Prakash et al. [19], as not all the phosphorus peaks detected in AlPO₄-41 are retained on manganese incorporation. In the case of ²⁷Al MAS NMR spectra two peaks are observed for AlPO₄-41 at $\delta = 42.5$ and 38.7 ppm, whereas only one peak is observed for MnAPO-41.

3.3. ESR studies

The X-band ESR spectrum of an Mn²⁺ ion ($S = 5/2$, $I = 5/2$) in a disordered state consists of six major lines due to the $m_S = |-1/2\rangle \leftrightarrow |+1/2\rangle$ transition, which is split into six lines due to hyperfine interaction with the manganese nucleus. The other transitions corresponding to $|\pm 5/2\rangle \leftrightarrow |\pm 3/2\rangle$ and $|\pm 3/2\rangle \leftrightarrow |\pm 1/2\rangle$ are usually not resolved due to a large anisotropy and they contribute to the background upon which the six major hyperfine lines are superimposed. Further, two small forbidden transitions due to $\Delta m_I = \pm 1$ appear between the adjacent hyperfine features [21,22]. These signals, which reduce the resolution

Table 2
TGA/DTA analysis of AlPO_4 and MnAPO_4 samples; weight loss and decomposition temperatures (K)

Sample	Weight loss (%) in stages ^a				
	I ^b	II	III	IV	V
AlPO_4 -41	6.8 [538] ^c (437–583) ^d	1.8 [653] (583–703)	tr [773] (703–873)	– – –	– – –
MnAPO -41 (iii)	6.0 [533] (433–606)	2.5 [631] (606–715)	tr [757] (715–823)	tr [880] (823–903)	tr [933] (sh) (903–983)
MnSAPO -41 (ii)	3.0 [499] (423–607)	0.5 [622] (607–673)	1.9 [733] (673–785)	2.4 [840] (785–1003)	tr [903] (sh)
AlPO_4 -11	5.5 [527] (441–595)	1.3 [631] (595–713)	1.2 [771] (713–883)	– – –	– – –
MnAPO -11	3.4 [513] (423–573)	tr [643] (573–673)	2.9 [743] (673–773)	2.7 [853] (773–973)	tr [903] (sh)

^a tr = trace; sh = shoulder.

^b Endothermic; other stages are exothermic.

^c Peak position, temperature (K).

^d Weight loss range, temperature (K).

of the overall spectrum, are noticeable when the zero-field splitting is non-negligible. The observed ESR spectra of $\text{MnAPO}(n)$ consist of a broad signal with characteristic Mn^{2+} hyperfine features superimposed on it. In general, the possible locations of Mn^{2+} in metal aluminophosphate molecular sieves are as follows:

- isolated Mn^{2+} ions in regular and defect (broken framework) aluminium sites;
- isolated Mn^{2+} ions in extra-framework locations;
- patches containing two or more Mn^{2+} ions occupying the nearby or adjacent aluminium positions; and
- small clusters of bulk MnO_x in the extra-framework locations.

While species (a) and (b) show ESR spectra with six major hyperfine lines typical for Mn^{2+} ions, the other two exhibit broad resonance features. The present study reveals the presence of all these possible species in MnAPO -11, MnAPO -41 and MnSAPO -41, their proportion depending on the type of aluminophosphate (11 or 41), the pH

of the gel used in synthesis (MnAPO -11, pH = 5.3; MnAPO -41, pH = 7.7) and the manganese content.

3.3.1. MnAPO -11

Fig. 4 shows the ESR spectra for the gel and powder samples of MnAPO -11. MnAPO -11(gel) shows six resolved hyperfine features at $g=2.003$ corresponding to isolated Mn^{2+} ions. The separation between the adjacent hyperfine lines is not equal and increases from 90 to 103 G, while the peak-to-peak line width (ΔH_{pp}) for individual hyperfine lines changes from 19.7 to 34.4 G in the direction of increasing field. The average hyperfine coupling constant (A_{Mn}) and peak-to-peak line width (ΔH_{pp}) are 96.7 G and 20.4 G, respectively. The as-synthesized sample of MnAPO -11 shows a spectrum similar to that of the gel, characteristic of isolated Mn^{2+} ions with $g_{iso}=2.004$. But distinct changes in hyperfine coupling constants and line widths are noticed for the crystalline samples compared with the gel. The gap between the adjacent hyperfine features increases from 72 to 110 G, while the line widths of individual hyperfine signals

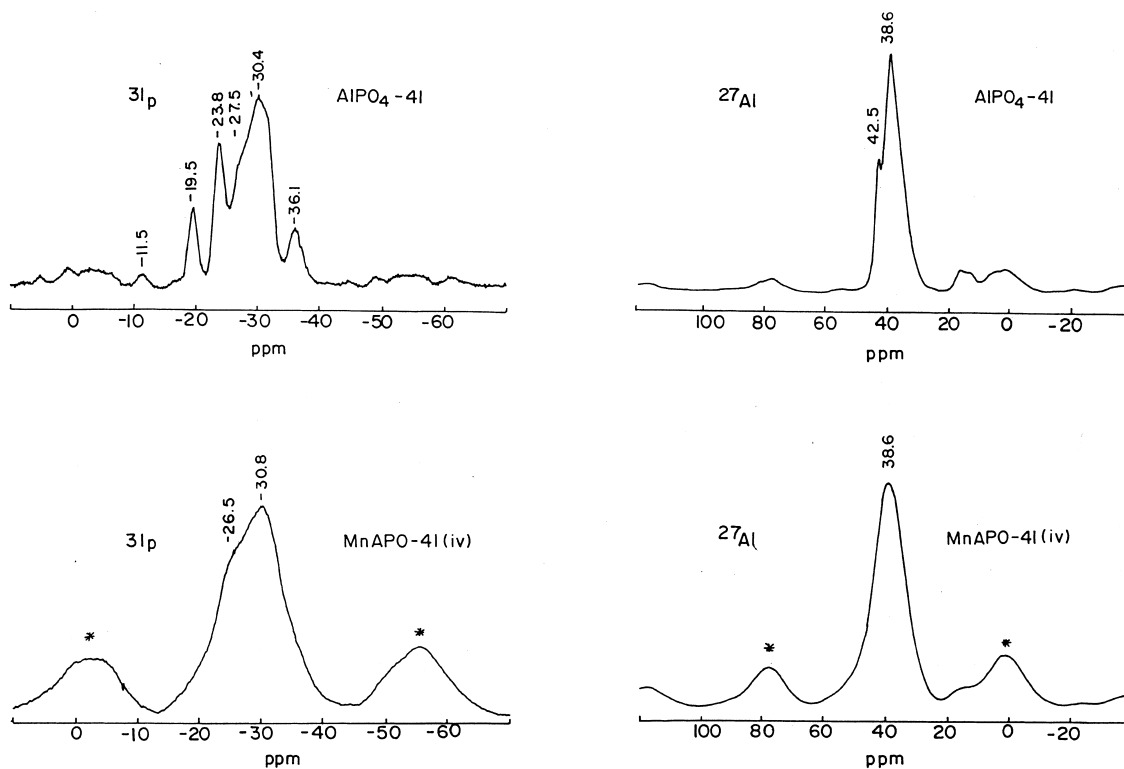


Fig. 3. ^{27}Al and ^{31}P MAS NMR spectra of $\text{AlPO}_4\text{-41}$ and MnAPO-41(iv) .

are broad and change from 37.5 to 75.5 G in the direction of increasing field. A_{Mn} and ΔH_{pp} for the as-synthesized sample are 90 G and 50 G, respectively. While intense, forbidden transitions are observed for the gel, the as-synthesized samples do not show these signals, indicating negligible zero-field splitting. Although the A_{Mn} values fall within the range reported for isolated Mn^{2+} ions, the larger line width (compared with extra-framework Mn^{2+} ions with O_h symmetry, 12–20 G for MnMCM-41 [23] and zeolites X and Y [24], as well as for the Mn^{2+} in the gel) suggests the location of the majority of Mn^{2+} in the as-synthesized sample to be the framework aluminium site, which is represented hereafter as species Ia'.

Calcined samples of MnAPO-11 showed a broad signal ($\Delta H_{\text{pp}}=500$ G) at $g=2.004$ (species II) and weak signals at $g_{\text{eff}}=4.27$ and 2.42 (species III). The overall normalized signal intensity measured by double integration for the calcined sample

is four times larger than that of the as-synthesized sample. The broad signal for species II is due to spin–spin interactions from the nearest neighbours. Although the signals due to isolated framework sites (species Ia) are not obvious from the spectrum, the second derivative spectral mode revealed their presence with a reduced hyperfine coupling constant of 85.4 G, probably due to dehydration and the lowering of symmetry to T_d . Similar observations on calcination were also reported by others for MnAPO-5 [11], MnAPSO-44 [14] and MnMCM-41 [23]. The additional broad signals at $g=4.27$ and 2.42 are attributed to isolated distorted tetrahedral framework sites (species III). Measurements at 77 K did not provide any additional information.

Exchanging the calcined sample with Na^+ ions and drying at 373 K did not change the ESR spectrum. The broad signal corresponding to species II and the moderately intense signals at $g=4.22$, 2.68 and 1.47 for species III are still the

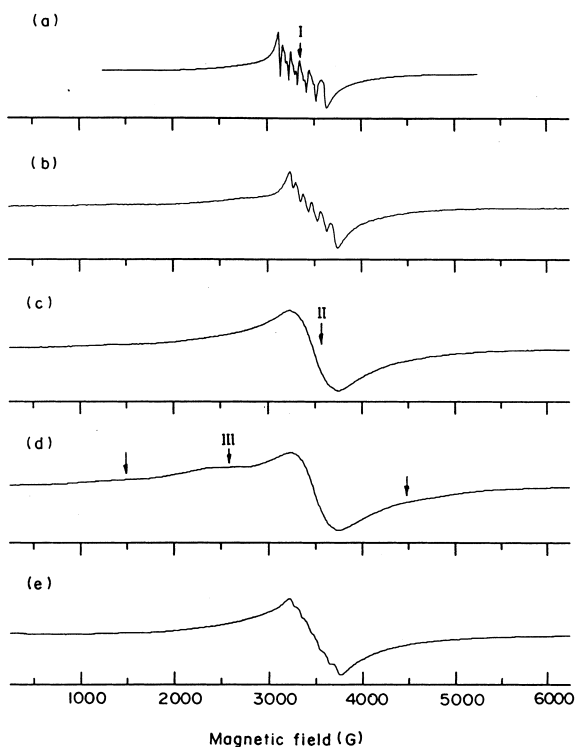


Fig. 4. X-band ESR spectra of MnAPO-11 gel (77 K) and the crystalline material (298 K) after various treatments: (a) gel, (b) as-synthesized, (c) calcined, (d) Na⁺-exchanged and calcined and (e) Na⁺-exchanged and hydrated samples. Species I–III are indicated in the figures.

main features of the spectra of the exchanged samples. The weak signal due to species III in the calcined sample becomes more dominant after Na⁺ exchange. Only a small fraction (7.4%) of the total manganese present in the calcined samples was removed on exchange with Na⁺ ions.

Rehydration of the Na⁺-exchanged sample (ambient atmosphere, relative humidity ~80%) regenerates partially the resolved sextet pattern corresponding to isolated framework substituted species I ($\Delta H_{pp} = 64$ G and $A_{Mn} = 96$ G). Moreover, the rehydrated samples showed a weak broad signal at $g \sim 15$ attributed to exchange-coupled Mn²⁺ hydrated clusters in the aluminophosphate structure (species IV), and these were not removed by Na⁺-ion exchange. This signal disappeared upon dehydration at 423 K for 16 h, suggesting an increase in spin–lattice relaxation of Mn²⁺ clusters

due to removal of the water. The ESR parameters and assignments for different Mn²⁺ species in MnAPO-11 are listed in Table 3. The values for species I and II agree well with those reported by Brouet et al. [13].

3.3.2. MnAPO-41

Typical spectra for MnAPO-41 gel and powder samples at various conditions are shown in Fig. 5 (sample MnAPO-41). While the MnAPO-11 gel shows a resolved sextet spectrum corresponding to isolated species, the MnAPO-41 gel, on the other hand, presents a broad signal at $g = 2.004$ with a peak-to-peak line width of 540 G and a weak set of six hyperfine features ($A_{Mn} \approx 90$ G) superimposed on the broad signal. As-synthesized samples of MnAPO-41 with 0.3 to 3% manganese in the initial gel exhibit similar ESR spectra to that of the gel sample. The second derivative spectrum for the sample with the lowest manganese content (0.3%) shows the presence of three isolated Mn²⁺ species (Ia, Ia' and Ib). Species Ib is characterized by the manganese hyperfine pattern with the separation between the adjacent lines increasing from 91 to 99 G, and an average A_{Mn} of 94.2 G. But for species Ia and Ia', this increase in separation with increasing field is from 60 to 111 G (average $A_{Mn} = 84.6$ G) and from 67 to 108 G (average $A_{Mn} = 88.6$ G), respectively. The g_{iso} values for these three species are 2.002, 2.002 and 2.004, respectively (Table 3). The values for species Ib match those of isolated Mn²⁺ with O_h symmetry in the extra-framework location [23,24] and Mn²⁺ ions in frozen solutions, whereas those of Ia and Ia' are similar to those of framework Mn²⁺ sites. At higher manganese contents, the spectra due to Ia, Ia' and Ib could not be resolved even in the second derivative mode probably because of larger Mn–Mn interactions broadening the signals.

It is to be noted that an aqueous solution of manganese acetate and dipropylamine above pH 7.0 shows a broad signal at $g \sim 2.0$ similar to that observed for the synthesis gel and crystalline sample of MnAPO-41. The origin of this broad signal in MnAPO-41 is therefore attributed to Mn(II)–template complexes occluded inside the pores.

Table 3
ESR parameters and assignments for different Mn^{2+} species in MnAPO-11, MnAPO-41 and MnSAPO-41 samples

Sample	Species	$g_{\text{iso/av}}$	ΔH_{pp} (G)	A_{Mn} (G)	Assignment and location
MnAPO-11	I	2.004	59	91	Distorted octahedral, framework
	II	2.004	500	Not resolved	Interacting Mn^{2+} ions in framework
	III	4.27, 2.42, 1.47	–	–	Distorted tetrahedral framework
	IV	~15	–	–	Extra-framework
MnAPO-41	Ia	2.002	–	94.2	Isolated octahedral extra-framework
	Ia'	2.002	–	84.6	Isolated hexa-coordinated framework
	Ib	2.004	–	88.6	Isolated hexa-coordinated framework
	II	2.004	540	Not resolved	Interacting Mn ions; mostly Mn–template complexes in cavities; extra-framework
	III	4.24, 2.54	–	–	Distorted tetrahedral framework
	IV	~15	–	–	Extra-framework
MnSAPO-41	Ia	2.002	–	95	Isolated Mn octahedral framework
	Ib	2.003	–	86	Isolated penta/hexa-coordinated, framework
	II	2.004	522	–	Patches and Mn–template complexes; framework/extra-framework

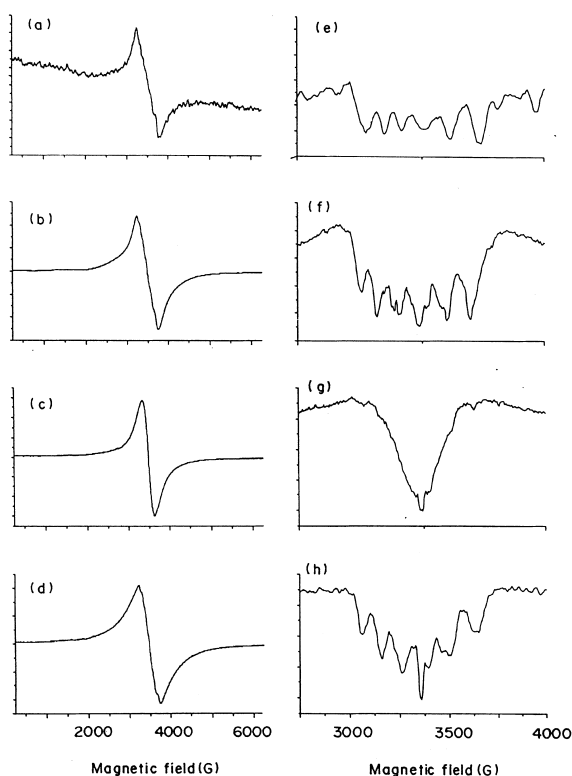


Fig. 5. ESR spectra of MnAPO-41(ii) gel with 0.3% manganese (77 K) and the crystalline material (298 K) after different treatments: (a) gel, (b) as-synthesized, (c) calcined and (d) calcined and rehydrated sample; (e), (f), (g) and (h) are the spectra in the second derivative mode for (a), (b), (c) and (d), respectively, revealing the presence of type I [isolated $\text{Mn}(\text{II})$] species.

MnAPO-41 shows dehydration and rehydration behaviour similar to that of MnAPO-11. Calcined and dehydrated samples of MnAPO-41 reveal a major broad signal (species II) at $g=2.008$ and weak signals (species III) at $g_{\text{eff}}=4.24$ and 2.54. Unlike MnAPO-11, the line width of the broad signal reduces considerably from 520 G for the as-synthesized sample to 290 G for the calcined and dehydrated sample. The overall intensity of the spectrum increased by about 2.5 times on calcination. The signals due to species Ia/a' and Ib are present even in calcined samples [Fig. 5(c)] but are broadened due to loss of hydrated water and changes in spin–lattice relaxation times. An additional sharp signal is seen in calcined samples at $g=2.0$. This is a paramagnetic carbon impurity from the burnt template.

Hydration of the calcined samples produces almost similar spectra to those of the as-synthesized samples, with the line width of the broad signal being 520 G. The signals at $g_{\text{eff}}=4.23$ and 5.24 attributed to distorted tetrahedral framework species are present even on rehydration.

3.3.3. MnSAPO-41

The overall intensity of manganese signals in the silicoaluminophosphate molecular sieve MnSAPO-41 is higher than in the corresponding MnAPO-41. A similar increase in manganese

content has also been reported for MnSAPO-5 [11], MnSAPO-44 [14] and MnAlMCM-41 [23]. Although the spectral features resemble that of MnAPO-41, the signals due to isolated Mn^{2+} ions are relatively more intense in MnSAPO-41 than in MnAPO-41. Two types of isolated Mn^{2+} species with $g_{\text{iso}}=2.0018$, $A_{\text{Mn}}=95$ G attributable to extra-framework sites (species Ib) and $g_{\text{iso}}=2.003$, $A_{\text{Mn}}=86$ G attributable to framework sites (species Ia) are present. The higher overall intensity of the ESR signal suggests that silicon enhances framework Mn^{2+} substitution in aluminophosphate type 41 structures. Similar framework substitutional effects by silicon were also observed by others in aluminophosphates of type 34 and 44 [8,14]. Rehydration of the calcined samples of MnSAPO-41 yields ESR spectra similar to those of the as-synthesized samples with well-resolved hyperfine pattern. Fig. 6 shows the spectra for

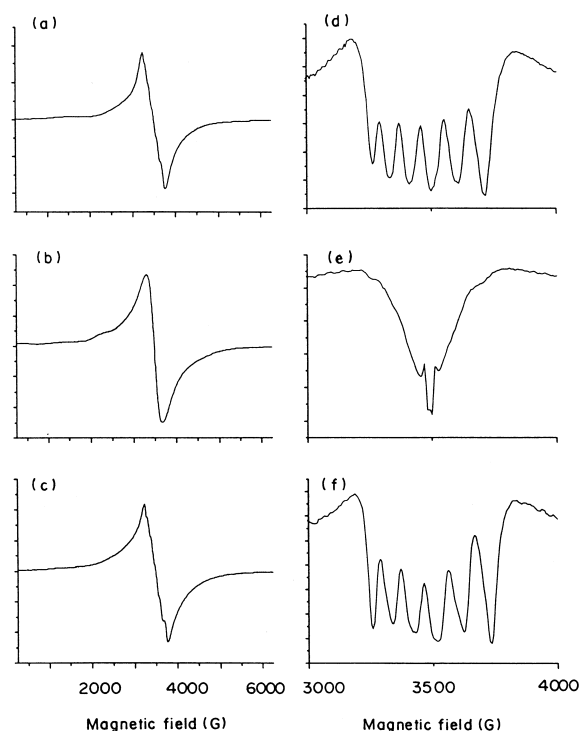


Fig. 6. ESR spectra of MnSAPO-41(ii) at 298 K. First derivative mode spectra for (a) as-synthesized, (b) calcined and (c) calcined and rehydrated samples. (d), (e) and (f) are the second derivative spectra of (a), (b) and (c), respectively, revealing the presence of type I [isolated $\text{Mn}(\text{II})$] species.

as-synthesized, dehydrated and hydrated forms of the MnSAPO-41(ii) sample. The assignment of various Mn^{2+} species in MnAPO-41 and MnSAPO-41 is given in Table 3.

Finally, ESR studies can only reveal $\text{Mn}(\text{II})$ species. The calcined samples possess larger ESR intensities than the as-synthesized samples, suggesting that significant transformation of $\text{Mn}(\text{II})$ into the (under the conditions of the ESR measurements) ESR-inactive $\text{Mn}(\text{III})$ species is unlikely. Nevertheless, it is possible that some $\text{Mn}(\text{III})$ species are formed during calcination.

4. Conclusions

Highly crystalline samples of MnAPO-11, MnAPO-41 and MnSAPO-41 could be synthesized using the same template, dipropylamine, and different hydrothermal synthesis conditions. TGA/DTA and ESR studies point to a greater framework substitution of manganese in the presence of silicon. The various Mn^{2+} species in the samples were identified as: (1) isolated Mn^{2+} in framework positions with both O_h and T_d symmetries, (2) patches of Mn^{2+} in the framework exhibiting Mn–Mn interactions, (3) isolated Mn^{2+} in extra-framework locations with O_h symmetry and (4) bulk MnO_x -type species outside the framework. The isolated framework Mn^{2+} species were present in larger amounts in MnAPO-11 than in MnAPO-41.

Acknowledgements

We thank Mrs. N.E. Jacob and Dr. S.S. Tamhankar for experimental help.

References

- [1] D. Barthomeuf, *Zeolites* 14 (1994) 394.
- [2] R. Vomscheid, M. Briend, M.J. Peltre, P.P. Man, D. Barthomeuf, *J. Phys. Chem.* 98 (1995) 9614.
- [3] B. Herreros, J. Klinowski, *J. Phys. Chem.* 99 (1995) 9514.
- [4] S. Ashtekar, C.V.V. Satyanarayana, D.K. Chakraborty, *J. Phys. Chem.* 98 (1994) 4878.
- [5] E.M. Flanigen, R.L. Patton, S.T. Wilson, in: P.J. Grobet,

- W.J. Mortier, E.F. Vansant, G. Schulz-Ekloff (Eds.), *Innovation in Zeolite Materials Science*, Studies in Surface Science and Catalysis vol. 37, Elsevier, Amsterdam, 1988, p. 13.
- [6] G.C. Bond, M.R. Gelsthrope, K.S. Sing, *J. Chem. Soc., Chem. Commun.* (1985) 1056.
- [7] E.M. Flanigen, B.M. Lok, R.L. Patton, S.T. Wilson, *Pure Appl. Chem.* 58 (1986) 1351.
- [8] S. Ashtekar, C.V.V. Satyanarayana, A.M. Prakash, D.K. Chakraborty, *J. Phys. Chem.* 100 (1996) 3665.
- [9] M. Mertens, J.A. Martens, P.J. Grobet, P.A. Jacobs, in: D. Barthomeuf, E.G. Derouane, W. Hölderich (Eds.), *Guidelines for Mastering the Properties of Molecular Sieves*, NATO ASI, Series B vol. 221, Plenum Press, New York/London, 1990, p. 1.
- [10] M. Hartmann, L. Kevan, *Chem. Rev.* 99 (1999) 635.
- [11] Z. Levi, A.M. Raitsimring, D. Goldfarb, *J. Phys. Chem.* 95 (1991) 7830.
- [12] C.W. Lee, X. Chen, G. Brouet, L. Kevan, *J. Phys. Chem.* 96 (1992) 3110.
- [13] G. Brouet, X. Chen, C.W. Lee, L. Kevan, *J. Am. Chem. Soc.* 114 (1992) 3720.
- [14] Z. Olender (Levi), D. Goldfarb, J. Batista, *J. Am. Chem. Soc.* 115 (1993) 1106.
- [15] D. Akolekar, R.F. Howe, in: H. Chon, S.-K. Ihm, Y.S. Uh (Eds.), *Progress in Zeolite and Microporous Materials*, Studies in Surface Science and Catalysis vol. 105, Elsevier, Amsterdam, 1996, p. 755.
- [16] A.M. Prakash, C.V.V. Satyanarayana, R.P. Bagwe, S. Ashtekar, D.K. Chakraborty, *Microporous Mater.* 6 (1996) 89.
- [17] C.A. Messina, B.M. Lok, E.M. Flanigen, US Patent No. 4 544 143, 1985.
- [18] P.S. Singh, R. Bandyopadhyay, B.S. Rao, *J. Chem. Soc., Faraday Trans.* 92 (1996) 2017.
- [19] M. Hartmann, A.M. Prakash, L. Kevan, *J. Chem. Soc., Faraday Trans.* 94 (1998) 723.
- [20] A.M. Prakash, M. Hartmann, L. Kevan, *J. Phys. Chem. B* 101 (1997) 6819.
- [21] T.I. Barry, L.A. Lay, *J. Phys. Chem. Solids* 27 (1966) 1821.
- [22] E. Meirovitch, R. Poupko, *J. Phys. Chem.* 82 (1978) 1920.
- [23] J. Xu, Z. Luan, T. Wasowicz, L. Kevan, *Microporous Mesoporous Mater.* 22 (1998) 179.
- [24] N.N. Tikhomirova, I.V. Nikolaeva, *Russ. J. Phys. Chem.* 55 (1981) 2224.